© 2017. Published by The Company of Biologists Ltd | Journal of Cell Science (2017) 130, 3116-3123 doi:10.1242/jcs.206979

RESEARCH ARTICLE

Engineering mammalian cells to seek senescence-associated secretory phenotypes

Anam Qudrat[1], Janice Wong[1] and Kevin Truong[1,2,*]

ABSTRACT

Since the removal of senescent cells in model organisms has been linked to rejuvenation and increased lifespan, senotherapies have emerged to target senescent cells for death. In particular, interleukin-6 (IL6) is a prominent senescence-associated secretory phenotype (SASP) and, thus, seeking IL6 could potentially localize engineered cells to senescent cells for therapeutic intervention. Here, we engineered a chimeric IL6 receptor (IL6Rchi) that generates a Ca^{2+} signal in response to IL6 stimulation. When IL6Rchi was co-expressed with an engineered Ca^{2+}-activated RhoA (CaRQ), it enabled directed migration to IL6 in cells that have no such natural ability. Next, the removal of target cells was accomplished by the mechanism of membrane fusion and subsequent death. This work represents a first step towards engineering a cell to target senescent cells that secrete high levels of IL6. For increased specificity to senescent cells, it will likely be necessary for an engineered cell to recognize multiple SASPs simultaneously.

KEY WORDS: IL6 receptor, IL6, Chimeras, Ca^{2+} signaling, Blebbing, Migration, Protein engineering, Synthetic biology

INTRODUCTION

Cells undergoing senescence not only exhibit arrest of cell proliferation, but also changes in protein expression and secretion that constitute the senescence-associated secretory phenotypes (SASPs) (Coppé et al., 2010). Interleukin-6 (IL6), a pleiotropic pro-inflammatory cytokine, is a prominent cytokine of SASP (Coppé et al., 2010). There are two main signaling pathways involving IL6: classic signaling and trans signaling (Calabrese and Rose-John, 2014; Scheller et al., 2011). In classic signaling, IL6 binds the IL6 receptor (IL6R) to induce the dimerization of the IL6R with gp130 (also known as IL6ST), a co-receptor that subsequently activates Janus kinases to modulate diverse processes, including metabolism, regeneration and neural processes (Boulanger et al., 2003; Calabrese and Rose-John, 2014; Scheller et al., 2011). In trans signaling, the complex of soluble IL6R and IL6 binds gp130 to induce similar downstream signaling. Owing to the prominent role of IL6 in SASP, IL6 secretion could potentially be used as an initial marker for senescent cells. Senotherapies target senescent cells for death either by apoptosis (i.e. senotopsis) or non-apoptotic death (i.e. senolysis), and the removal of senescent cells in model organisms (e.g. mice) has extended healthy life span (Baker et al., 2016, 2011). Protein-based or chemical drugs used as senotherapies (e.g. the cancer drug dasatinib) are often administered systemically and thus have nonspecific targeting risks (Childs et al., 2015). Alternatively, if cells can be engineered to seek IL6 sources (e.g. potential sites of senescent cells) to locally deliver a therapeutic intervention, such risks can potentially be avoided. Furthermore, these engineered cells could further recognize the microenvironment of the senescent cells by local inflammation, which has a characteristically low pH (Bellocq et al., 1998; Castro-Vega et al., 2015; Naghavi et al., 2002; Van Overmeire et al., 2016).

Certain cell types, such as monocytes and T cells, can naturally migrate towards IL6 sources through chemoattractant signaling that involves complex signaling interactions of many co-receptors, adaptor proteins and signaling proteins, which may not be ubiquitously expressed or are much less known (Luster et al., 2005). The ability to program cells with no natural migratory potential to IL6 sources (e.g. HEK293 cells) would widen cell therapy options. Synthetic biosystems for controlling cell migration involve engineering control over RhoA or Rac1 small GTPases because of their central role in regulating cytoskeletal rearrangement within cells (Guo et al., 2012; Mills et al., 2012; Mills and Truong, 2011; Wu et al., 2009). In particular, our group engineered a Ca^{2+}-activated RhoA protein (named CaRQ) to allow Ca^{2+}-mediated cellular bleb formation (Mills and Truong, 2011) and a Ca^{2+}-activated Rac1 protein (named Racer) to allow Ca^{2+}-mediated lamellipodia formation (Mills et al., 2012). The major advantage of these Ca^{2+}-activated synthetic proteins is that they allow the rewiring of any receptor that generates a Ca^{2+} signal to cell migration towards that receptor's target ligand. For example, because vascular endothelial growth factor (VEGF) binding to VEGF receptor 2 (VEGFR2) generates a Ca^{2+} signal, a cell co-expressing CaRQ and VEGFR2 allows migration directed by VEGF (Mosabbir and Truong, 2017). As not all receptors generate a Ca^{2+} signal upon binding their target ligand, we developed an approach to engineer chimeric receptors that would generate a Ca^{2+} signal by replacing the natural cytoplasmic domain with the cytoplasmic domain of VEGFR2 (Qudrat and Truong, 2017).

The binding of IL6 to the IL6R induces a Ca^{2+} signal in various types of neurons of the digestive system (Anesten et al., 2016; O'Malley et al., 2011), but suppresses Ca^{2+} signals in other types of cells, such as cardiomyocytes (Smart et al., 2006). This is consistent with the pleiotropic effect of IL6 as it is exhibits opposite Ca^{2+} effects in different cell types or contexts. To allow the robust generation of a Ca^{2+} signal upon binding to IL6, we first engineered IL6Rchi (a chimeric IL6R) by fusing the extracellular domain of the IL6R with the transmembrane and cytoplasmic domain of VEGFR2. Next, the Ca^{2+} signal from IL6Rchi was rewired to cell migration by co-expression with our Ca^{2+}-activated RhoA protein (CaRQ) (Mills and Truong, 2011), which in effect rewired cellular blebbing to IL6 stimulation. When co-culturing the IL6-expressing

[1]Institute of Biomaterials and Biomedical Engineering, University of Toronto, 164 College Street, Toronto, Ontario, M5S 3G9, Canada. [2]Edward S. Rogers, Sr. Department of Electrical and Computer Engineering, University of Toronto, 10 King's College Circle, Toronto, Ontario, M5S 3G4, Canada.

*Author for correspondence (kevin.truong@utoronto.ca)

J.W., 0000-0002-6951-7396; K.T., 0000-0002-9520-2144

Received 1 June 2017; Accepted 25 July 2017

Journal of Cell Science (2017) 130, 3116-3123 doi:10.1242/jcs.206979

cells (i.e. an IL6 source) with our engineered IL6Rchi- and CaRQ-expressing cells (i.e. IL6-seeking cells), the IL6-seeking cells showed directional displacement towards the IL6 source cells. Lastly, because local and chronic inflammation often precedes the development of SASP, the microenvironment of senescent cells is also associated with a low pH (Coppé et al., 2010). By adding vesicular stomatitis virus glycoprotein G (VSVG) and herpes simplex virus type 1 thymidine kinase (TK) into these IL6-seeking cells, the cells can perform cell-to-cell membrane fusion upon low pH induction (Nagaraj et al., 2013) and cell death upon ganciclovir (GCV) drug treatment (Kokoris and Black, 2002), respectively.

RESULTS

IL6 triggers a Ca^{2+} signal in a synthetic chimera

When stimulated with IL6, a Ca^{2+} signal was generated by a chimeric protein consisting of IL6R and VEGFR2. This chimera, named IL6Rchi, was constructed by the tandem fusion of the extracellular domain of IL6R with the transmembrane and cytoplasmic domains of VEGFR2 (Fig. 1A). Previously, we developed an approach to engineer chimeric receptors that would generate a Ca^{2+} signal by replacing the natural cytoplasmic domain with the cytoplasmic domain of VEGFR2 (Qudrat and Truong, 2017). The only requirement is that binding of the target ligand on the extracellular domain of the natural receptor induces oligomerization, because this causes the corresponding oligomerization of the fused cytoplasmic domain of VEGFR2, which in turn recruits phospholipase C to initiate inositol triphosphate (IP_3)-mediated Ca^{2+} release from the endoplasmic reticulum. As IL6R oligomerization with IL6 is supported by both biochemical and structural data (Boulanger et al., 2003; Calabrese and Rose-John, 2014; Scheller et al., 2011), a similar replacement of the cytoplasmic domain with VEGFR2 was expected to be effective in robustly generating a Ca^{2+} signal.

Lentiviral infection of the SINp-detector transfer vector in HEK 293 cells under zeocin selection generated a stable cell line called the IL6 detector cells. The detector cells expressed both the IL6Rchi and the red Ca^{2+} sensor RCaMP1.07 (Ohkura et al., 2012) (Fig. S1A). RCaMP1.07 labeled the plasma membrane (PM) through tyrosine protein kinase Lyn (Lyn) (^{1}MGCIKSKGKDSA^{12}), which localizes to the cytoplasmic side of the PM following palmitoylation of the cysteine amino acid (Fig. 1A). A dim red fluorescence outlines the cell periphery showing this PM localization (Fig. 1B). Bolus addition of 10 ng/ml IL6 to the extracellular medium of the IL6 detector cells triggered a Ca^{2+} signal, lasting ~30.8±4.9 s, which was comparable to that resulting from activation by ATP, a positive control (Fig. 1C,D; Fig. S1B and Movie 1). A second Ca^{2+} signal was triggered by another IL6 stimulation of these detector cells (Fig. S1C). Control cells expressed only RCaMP1.07 or VEGFR2tail alone (i.e. no IL6R component) and neither showed a Ca^{2+} response to IL6 stimulation (Fig. 1D). To abolish the Ca^{2+} signal, the IL6 detector cells were pre-incubated with 50 nM staurosporine (STS) because STS is a broad spectrum kinase inhibitor that inhibits phosphorylation required for recruiting phospholipase C and thus inhibits the Ca^{2+} signal (Rüegg and Burgess, 1989). As expected, when the IL6 detector cells were stimulated with IL6 after pre-incubation with STS, no Ca^{2+} response was observed (Fig. 1D). Moreover, the IL6 detector cells did not generate a Ca^{2+} signal when stimulated with more media (i.e. PBS)

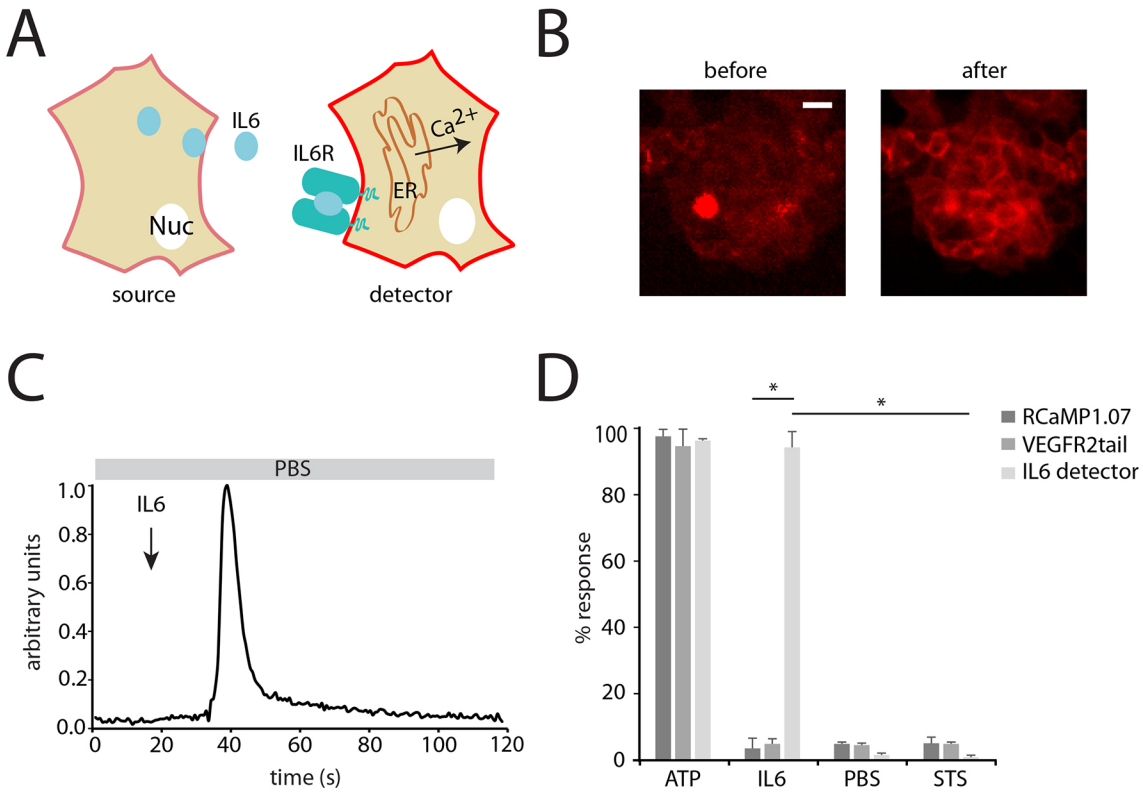

Fig. 1. In IL6 detector cells expressing the red Ca^{2+} sensor RCaMP1.07 (labeling the PM) and chimeric IL6 receptor (IL6Rchi), a Ca^{2+} signal is triggered in response to extracellular IL6. (A) Schematic of the mechanism of activation of IL6Rchi. (B) Representative images showing IL6 detector cells expressing RCaMP1.07 and IL6Rchi stimulated with 10 ng/ml IL6, showing the dim (before) and bright (after) outline of the cell periphery (mCherry, red). Scale bar: 20 µm. (C) Representative Ca^{2+} trace observed with 10 ng/ml IL6 in IL6 detector cells. (D) Percentage cell response in IL6 detector cells compared with cells expressing only the VEGFR2tail or RCaMP1.07 stimulated with 10 µM ATP, 10 ng/ml IL6 or 50 nM STS. Data are mean±s.d. *P<0.01 (one-factor ANOVA followed by a Tukey-Kramer post-hoc test). All experiments were repeated at least three times, with 12 cells per trial. See also Fig. S1 and Movie 1.

Journal of Cell Science (2017) 130, 3116-3123 doi:10.1242/jcs.206979

(Fig. 1D). Thus, IL6 detector cells generated a Ca^{2+} signal when stimulated with IL6.

IL6 triggers dynamic blebbing in a synthetic chimera, allowing it to seek IL6 sources

Lentiviruses were created using the SINp-seeking transfer vector and infected into HEK293 cells (Fig. S1A). Under zeocin selection, this generated a stable cell line, called the IL6-seeking cells, expressing both IL6Rchi and CaRQ. As CaRQ was labeled to the PM and fused to Venus (yellow fluorescent protein mutant), it was visible in the IL6-seeking cells by the yellow fluorescent outline of the cell periphery (Fig. 2A). As expected, the addition of 10 ng/ml IL6 triggered dynamic blebbing in IL6-seeking cells (n=3 independent experiments) (Fig. 2B,C). The blebs protruded and retracted at an average velocity of 1.11±0.5 µm/min, with an average bleb diameter of 2.18±0.6 µm and an area of 3.93±2.2 µm^2 (Fig. 2C; Movie 2). Blebbing significantly diminished (n=3 independent experiments, P<0.01) when the IL6-seeking cells were pre-incubated with 1 µM Y-27632 (a ROCK I and II inhibitor) (Liao et al., 2007) (Fig. 2D). Hence, IL6 triggered dynamic blebbing in IL6-seeking cells.

The IL6-seeking cells used amoeboid-like blebbing as a migratory mode to seek IL6 source cells. To generate a synthetic IL6 source *in vitro*, a stable HEK293 cell line was created with the lentiviral infection of the SINp-source transfer vector under blasticidin selection (Fig. S1A). This cell line, called the IL6 source cells, expressed both IL6 and the PM-labeled mCherry fluorescent protein (named LynCherry). A 1 hour time lapse showed an IL6-seeking cell moving towards the IL6 source cell (Fig. 2E; Movie 3) at velocities averaging 44.7±4.7 µm/h (Fig. 2F). The seeking cells appeared round because they were strained into single cells prior to plating. Single cells exhibited increased motility because, unlike clusters, they do not need to detach from the substrate or their neighbors before moving towards the source. Control cells, called null cells, were generated using the SINp-null transfer vector under blasticidin selection and expressed the PM-labeling Cerulean fluorescent protein (named LynCeru) (Fig. S1A). When null cells were co-cultured with the source cells, there was no physical displacement towards the source cells (Fig. 2F).

IL6-seeking cell populations undergo directed migration to seek IL6 source cells

Over longer time courses of several days, the IL6-seeking cells moved towards the IL6 source cells in characteristic spatial patterns. When a cluster of seeking cells was co-cultured with a cluster of source cells, the seeking cells separated from their cluster and made cell-cell contact with the source cluster, often accumulating at its periphery (Fig. 3A). In control cases with seeking and null clusters, no such characteristic was seen because the clusters grew independently in a radial fashion even when they were very near to each other (Fig. 3A). We defined this feature as ‘surround’ and used two metrics to quantify it: % edge coverage and % edge cross. Observation of clusters 2 days after co-incubation showed 73±5.6% edge coverage and 47.7±18.9% edge cross; both measures were significantly (mean±s.d., n=3, P<0.01) higher than those of the control case (Fig. 3B). The null cells showed significantly (P<0.01) less % edge coverage and % edge cross than source cells (Fig. 3B). The breakage and directional spread of the IL6-seeking cells towards the source cluster was seen in rose diagrams over a 2-day observation period (n=3, P<0.01) (Fig. 3C; Fig. S2A).

To further quantify chemotaxis to IL6, conventional transwell assays were conducted. When the IL6-seeking cells were plated in the apical chamber of the wells, they showed significant (n=3, P<0.01) migration towards the IL6 source cells plated in the basal chamber, but not towards the null cells (Fig. 3D). Further, stimulation with IL6 or ATP resulted in a significantly (n=3, P<0.01) larger percentage of the IL6-seeking cells migrating across the thin membrane compared to a ROCK I/II inhibitor (Y-27632) (Fig. 3D). To show that the effect was not chemokinesis or random movement due to IL6, IL6 was added to both the apical and basal chambers of the transwell. In this condition, the IL6-seeking cells did not significantly migrate across the thin membrane (Fig. 3D). Further, IL6-seeking cells migrated towards two examples of senescent cells (Fig. S2B). While MDA-MB-231 breast cancer cells can spontaneously undergo senescence (Cukusic et al., 2006), HeLa cells can enter a senescent state after TNFα stimulation (Hubackova et al., 2016). Thus, IL6-seeking cells migrated towards IL6 sources.

Additional genes allow IL6-seeking cells to fuse with source cells and undergo death

With the addition of the VSVG and TK genes, the IL6-seeking cells first gained the ability to undergo membrane fusion with source cells at low pH forming multinucleated fused cells called syncytia (Nagaraj et al., 2013), and second gained the ability to subsequently kill these syncytia with GCV treatment (Fig. 4A). This property could be useful for recognizing the low pH microenvironment of senescent cells associated with chronic and local inflammation (Bellocq et al., 1998; Castro-Vega et al., 2015; Naghavi et al., 2002; Van Overmeire et al., 2016). Lentiviral infection of the IL6-seeking cells with the SINp-fuse transfer vector created a stable cell line named the IL6-seeking (+ fuse) cells (Fig. S1A). While CaRQ was visible by a yellow fluorescent outline on the cell periphery, cyan fluorescence in the cytoplasm indicated the presence of VSVG, which expressed Cerulean with a C-terminal nuclear export signal (or CeruNES) (Fig. S1A). Similarly, the IL6-seeking (+ fuse) cells retained the ability to seek the IL6 source cells in transwell experiments (Fig. 4B). Twenty-four hours after a 1 min induction with the low pH (6) of the IL6-seeking (+fuse) cells, membrane fusion of the source and seeking (+fuse) cells was evident by the appearance of syncytia displaying all three fluorescent proteins: red from LynCherry, yellow from CaRQ and cyan from CeruNES (Fig. 4C). Lastly, the IL6-seeking (+fuse) cells underwent cell death by GCV. TK-modified GCV is incorporated into genomic DNA, where it causes DNA instability, cell cycle arrest and, ultimately, caspase-9-dependent apoptosis (Tomicic et al., 2002). Hence, the syncytia were eliminated post-treatment with 50 µM GCV over a 7 day period. TK/GCV-mediated death was observed in the timescale of weeks (depending on the cell line) in Beck et al. (1995); however, significant death was observed after 3 days in our experiments. The number of syncytia significantly reduced (n=3, P<0.01) as compared with no treatment controls (Fig. 4D).

DISCUSSION

To enable cell-based senotherapies, it is necessary to first engineer cells to seek SASPs, of which IL6 secretion is a prominent phenotype (Coppé et al., 2010). Although some specific cell types of the immune system naturally seek IL6, we have engineered this ability into cells (i.e. HEK293) that do not naturally seek IL6, allowing more options in cell-based therapy. Specifically, we first engineered the IL6Rchi to robustly generate a Ca^{2+} signal upon IL6 stimulation. This Ca^{2+} signal triggered blebbing via CaRQ, which allowed for migration towards IL6 sources. Unlike protein-based or chemical drugs, cells have many options for localized treatment, such as secretion of therapeutic proteins (e.g. monoclonal antibodies or cytokines), differentiation into particular cell types, or fusion and

Journal of Cell Science

Journal of Cell Science (2017) 130, 3116-3123 doi:10.1242/jcs.206979

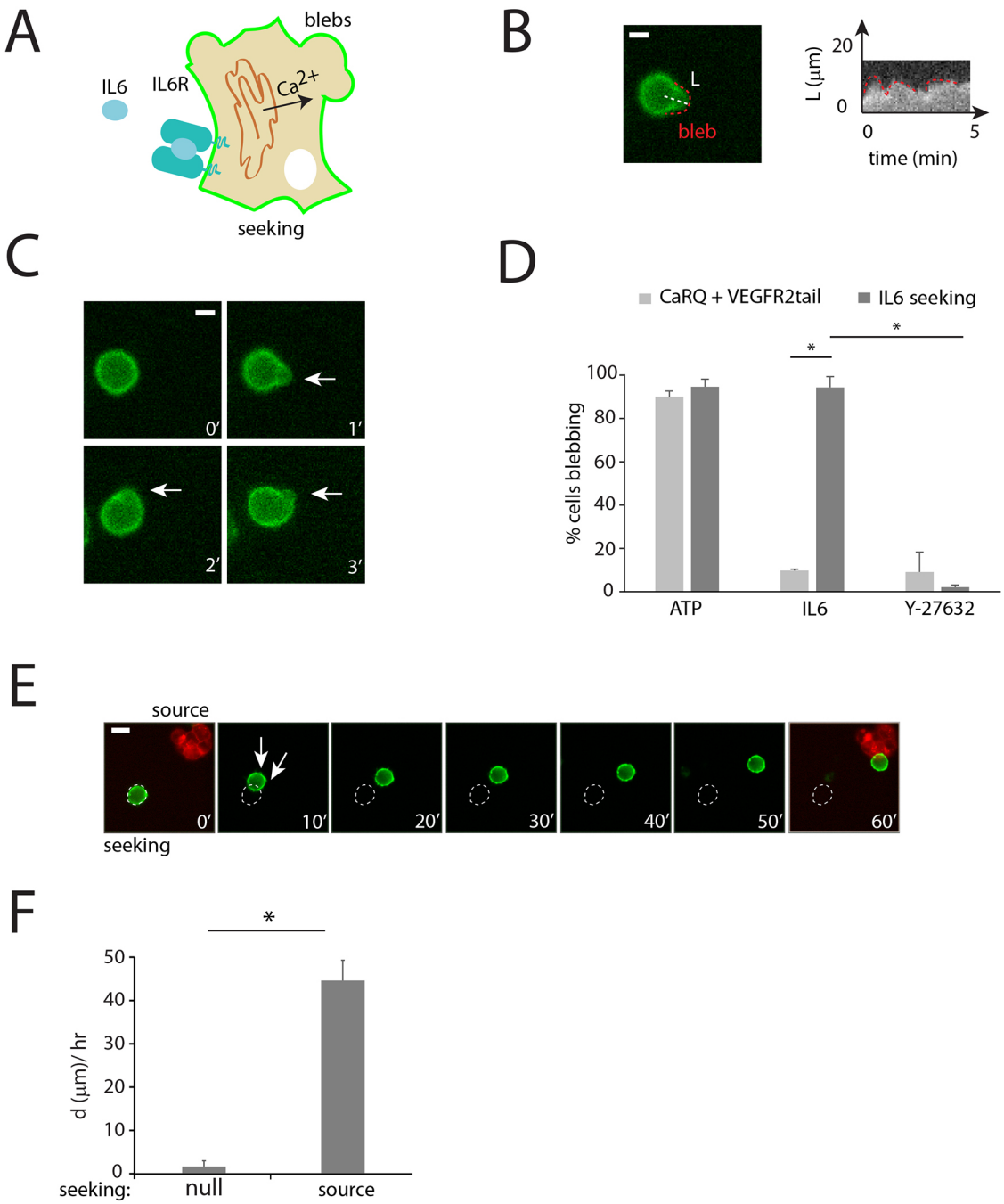

Fig. 2. IL6-seeking cells expressing IL6Rchi and CaRQ dynamically bleb and migrate to the IL6 source when stimulated with IL6. (A) Schematic of the activation mechanism of the IL6Rchi and CaRQ system. (B) Representative kymograph showing blebbing kinetics along line L, running from the middle of the cell to the bleb extremity. The red dashed line traces a bleb expanding and retracting orthogonal to the cell body (Venus, green). Scale bar: 20 µm. (C) Images showing Venus fluorescence of CaRQ expression from the IL6-seeking cells. Post-stimulation with 10 ng/ml IL6, images captured at t=0, 1, 2 and 3 min show blebs forming, protruding/growing in size and retracting. Scale bar: 20 µm. (D) Percentage of IL6-seeking cells blebbing compared with cells transfected with only the VEGFR2tail or CaRQ stimulated with 10 µM ATP or 10 ng/ml IL6, or following 30 min incubation with 1 µM Y-27632 (a ROCK I/II inhibitor). Data are mean±s.d. *P<0.01 (one-factor ANOVA followed by a Tukey-Kramer post-hoc test). All experiments were repeated at least three times, with nine cells per trial. (E) Images of an IL6-seeking cell co-cultured with an IL6 source cell, showing displacement of the seeking cell towards the source cell at 10 min intervals. The first and last frames show merged channels. Arrows indicate small blebs (mCherry, red; YFP, green). Scale bar: 10 µm. (F) Displacement of an IL6-seeking cell to a source cell over a 1 h time-lapse. Data are mean±s.d. *P<0.01 (Student's t-test); n=3, with three cells per trial. See also Movies 2 and 3.

subsequent death, as presented in this study. Given the pleiotropic effects of IL6, seeking sites of IL6 secretion are likely not specific enough to only seek senescent cells. With more research in SASPs to discover more specific signaling cues, it is possible to rewire migration to other signaling cues using the engineering strategy presented in this study. Alternatively, we could engineer the cell to recognize a combination of SASPs that together are specific to senescent cells. Similar to IL6Rchi, chimeric receptors could be assembled for other SASPs [e.g. IL8 (also known as CXCL8) and HGF] (Coppé et al., 2010) and added together into the engineered

Journal of Cell Science (2017) 130, 3116-3123 doi:10.1242/jcs.206979

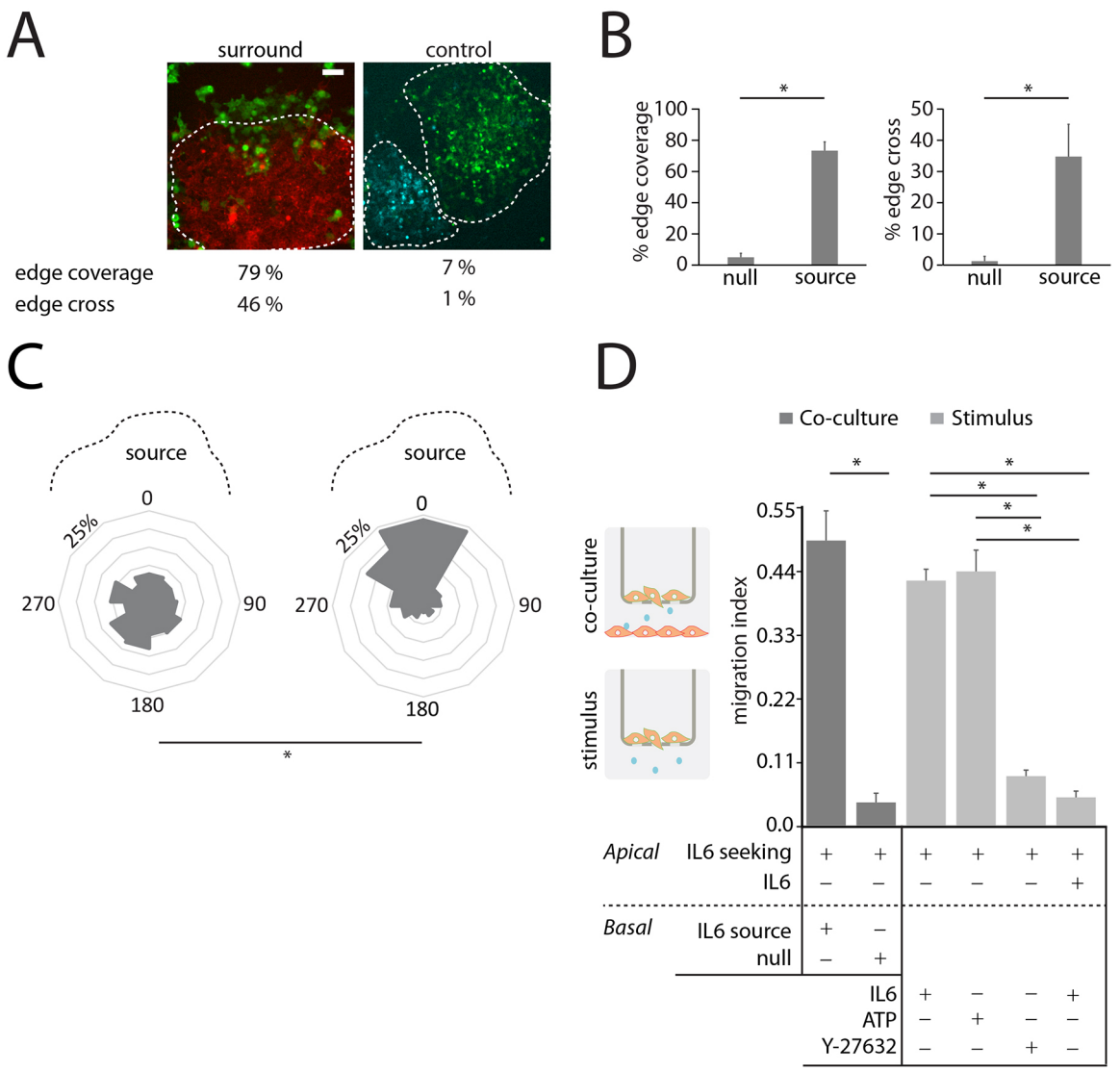

Fig. 3. IL6-seeking cells show autonomous migration towards IL6 sources. (A) Images of IL6-seeking cells co-cultured with a cluster of IL6 source cells showing 'surround'. Control null cells show no characteristic feature when co-cultured with source cells (mCherry, red; Cerulean, cyan; YFP, green). Dashed line shows the outline of the source cluster. Scale bar: 100 µm. (B) Quantification of the 'surround' phase with % edge coverage and % edge cross metrics. *P<0.01 (Student's t-test); n=6 clusters. (C) Rose plots of the spatial distribution of IL6-seeking cells on Day 1 (left) and 2 (right) post-incubation with IL6 source cluster. *P<0.01 (Watson's two-sample test of homogeneity); n=6 clusters. (D) Transwell experiments (schematic on the left) showing cell migration in response to co-culturing with synthetic cell lines (i.e. IL6 source and null) or stimuli (i.e. 10 ng/ml IL6, 10 µM ATP, or 1 µM Y-27632). *P<0.01 (one-factor ANOVA followed by a Tukey-Kramer post-hoc test). All experiments were repeated at least three times.

cell. Locations with the combination of SASPs should induce more Ca^{2+} signal generation and, consequently, more robust cell migration.

With the aim of reducing off-target effects, other senolytic therapies now moving toward clinical trials are targeting cellular pathways that have greater specificity to senescent cells (Saraswat and Rizvi, 2017). When cells of our immune system (i.e. monocytes, macrophages, neutrophils and T lymphocytes) are functioning at their best, they embody the characteristics of the ideal therapeutic because they adeptly detect disease conditions and then respond specifically and locally to minimize systemic side effects. Indeed, the best approach to cell-based senotherapy may be to add engineered genes for incremental functions to these immune cells, as exemplified by CAR T cells, in which a chimeric T-cell receptor for CD19 was added to T lymphocytes collected from patients (Kalos et al., 2011). We anticipate our system of engineered proteins could similarly be added to collected monocytes or pluripotent stem cell-derived monocytes. These engineered monocytes could be intravenously injected where they would naturally accumulate at sites of vascular inflammation through endogenous expression of P-selectin ligand, and then selectively extravasate to sites of senescent tissue through our engineered SASP-seeking system. Although the sites near the vasculature of senescent tissue should not accumulate low pH because of capillary blood flow, the engineered monocytes that extravasate deeper into the senescent tissue could potentially experience low pH from the hypoxia and chronic inflammation. This low pH could then, in turn, activate VSVG for the delivery of the TK/GCV-mediated cell death that kills both our engineered and targeted senescent cells.

MATERIALS AND METHODS

Cell lines

Human embryonic kidney (HEK293), MDA-MB-231 and HeLa cells were maintained in Dulbecco's modified Eagle's medium containing 25 mM

Journal of Cell Science (2017) 130, 3116-3123 doi:10.1242/jcs.206979

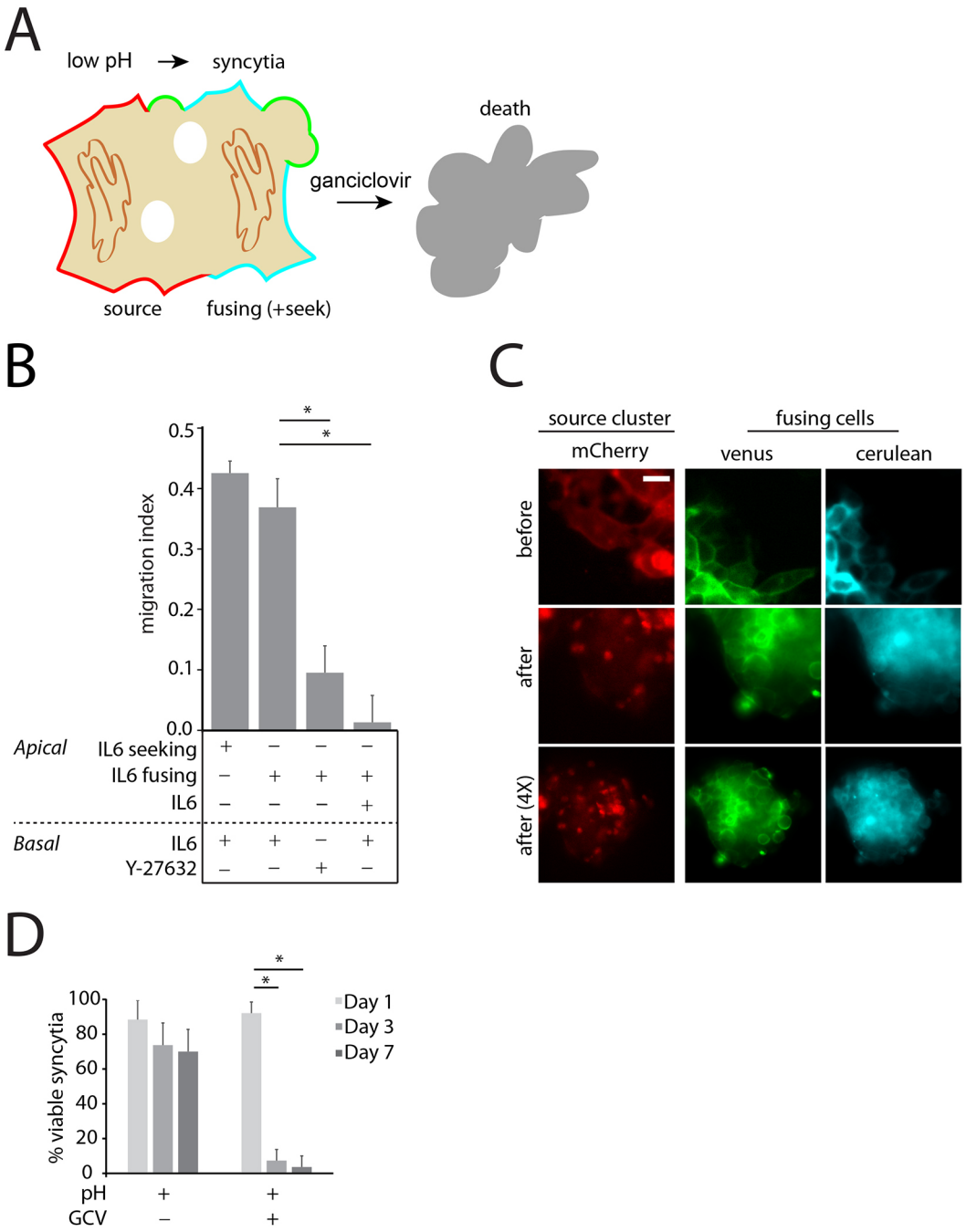

Fig. 4. IL6-seeking (+fuse) cells expressing IL6Rchi, CaRQ and VSVG cells seek and fuse with IL6 sources upon low pH induction. (A) Schematic of the mechanism of activation of the IL6-seeking (+fuse) cells. (B) Transwell experiments showing IL6-seeking (+fuse) cell migration in response to stimulation with 10 ng/ml IL6 or 1 µM Y-27632. *P<0.01 (one-factor ANOVA followed by a Tukey-Kramer post-hoc test). All experiments were repeated at least three times. (C) Representative images showing IL6-seeking (+fuse) cells fusing with the IL6 source cell cluster after low pH induction (mCherry, red; YFP, green; Cerulean, cyan). Scale bar: 10 µm. (D) Percentage of viable syncytia after 7 day treatment with 50 µM GCV following low pH induction. Data are mean±s.d. *P<0.001 (one-factor ANOVA followed by a Tukey-Kramer post-hoc test); n=3, with nine syncytia per trial.

D-glucose, 1 mM sodium pyruvate and 4 mM L-glutamine (Invitrogen), supplemented with 10% fetal bovine serum (Sigma-Aldrich), in T25 flasks (37°C and 5% CO_2). All cell lines were authenticated and tested for contamination. Cells were passaged at 90% confluency using 0.05% TrypLE with Phenol Red (Invitrogen) and seeded onto 24-well plates (Corning) at 1:20 dilution. Cells were transiently transfected using Lipofectamine 3000, according to the manufacturer's protocols (Invitrogen). Then, 24 h post-transfection, cells were treated with 0.05% TrypLE with Phenol Red (Invitrogen) and plated in six-well tissue culture plates (Corning) at a serial dilution, 1:2, 1:4, 1:8, 1:16 and 1:32. All stable HEK 293 cell lines were generated by lentiviral infection using the respective SINp transfer vector and subsequent selection with blasticidin (10 µg/ml), puromycin (1 µg/ml) or zeocin (200 µg/ml) for 2 weeks. Colonies were plated in 96-well tissue culture plates (Sarstedt) for subsequent experiments and imaging.

Cell stimulation

Colonies plated in 96-well tissue culture plates were washed with PBS and imaged in serum-free media (Thermo Fisher Scientific). Subsequently, 10 ng/ml IL6 (BioAspect), 20 ng/ml TNFα (BioAspect) or 10 µM ATP

(Sigma-Aldrich) was added as a bolus. Membrane fusion was achieved by incubating cells in PBS (pH 6) for 1 min. 50 µM GCV (Sigma-Aldrich) was added for a 7 day period to observe syncytia decline and cell death. To inhibit Ca^{2+} signals or blebbing, cells were pre-incubated for 30 min in PBS with 50 nM STS (Sigma-Alrich) or 1 µM Y-27632 (Sigma-Aldrich), respectively. Cells were stained with Trypan Blue (Sigma-Aldrich) and counted using INCYTO C-Chip disposable hemacytometers (Fisher Scientific). Transwell experiments were performed with ThinCert cell culture inserts (Greiner Bio-One), following the manufacturer's protocol. The migration index was calculated by dividing the number of cells that had migrated (bottom side of the membrane) by the total number of cells.

Plasmid construction

The transfer vectors SINp-detector, SINp-source, SINp-null, SINp-seeking and SINp-fuse were synthesized by Genscript and subcloned into the pUC57-Simple vector using EcoRV. IL6Rchi was synthesized as the tandem fusion of the extracellular domain of the IL6 receptor (amino acids 1–365) and the transmembrane and cytoplasmic domain of VEGFR2 (amino acids 765–1356). LynCherry or LynCerulean (LynCeru) was synthesized as the tandem fusion of the signal sequence of Lyn (^{1}MGCIKSKGKDSA^{12}) with mCherry or mCerulean. CeruNES was synthesized as the tandem fusion of mCerulean and the nuclear export signal (^{1}LQLPPLERLTLD^{12}) from the HIV-1 Rev protein. IL6 (amino acids 1–212), vesicular stomatitis virus glycoprotein G (VSVG) (amino acids 1–511) and CaRQ were synthesized by Genscript. All genes were highly expressed with the cytomegalovirus promoter (CMVp) in mammalian cells. All plasmid manipulations were performed by Genscript. All plasmids were transformed in *E. coli DH5-α* and isolated using a Mini-prep kit (Invitrogen).

Illumination and imaging

Imaging was performed using an inverted IX81 microscope with a Lambda DG4 xenon lamp source and a QuantEM 512SC CCD camera with a 10× or 40× objective (Olympus). Filter excitation (EX) and emission (EM) bandpass specifications (in nm) were as follows: CFP (EX, 438/24; EM, 482/32), YFP (EX, 500/24; EM, 542/27), RFP (EX, 580/20; EM, 630/60) (Semrock). Image acquisition and analysis were performed with µManager and ImageJ software, respectively (Edelstein et al., 2014; Schneider et al., 2012).

Data quantification

The Ca^{2+} signal was measured using the Live Intensity Plot plugin for ImageJ. The duration of the signal was manually measured between the rise and back-to-basal level of the trace. The signal intensity was normalized between 0 and 1, using the formula $x_{max} = \frac{x - x_{min}}{x_{max} - x_{min}}$, and reported as arbitrary units. The 'surround' pattern of the seeking cells around the source cluster was quantified using the % edge overlap and % edge cross metric. To calculate these metrics, traces of the leading edge/front of the seeking cells and the source/null cluster were manually drawn. For % edge overlap, these two lines were transposed on each other and the degree of overlap was calculated between the two lines. For % edge cross, the number of cells inside the boundary over the total number of cells in the area of observation was calculated.

Statistical analysis

All experiments with n=3 were conducted three times independently with at least nine cells evaluated in each trial. All data with normal distribution and similar variance were analyzed for statistical significance using two-tailed, unpaired Student's *t*-tests, unless otherwise indicated. Multiple group comparisons were made with one-factor ANOVA with Tukey-Kramer post-hoc test. For all tests, α was set at 0.05. P<0.05 was considered significant. Data are mean±s.d. unless otherwise stated. Data were analyzed using Real Statistics Resource Pack for Excel (Microsoft). Comparison of migration direction was performed using Watson's two-sample test of homogeneity using the CircStats package, and spatial distributions were analyzed using SpatStat in R software (R Development Core Team).

Competing interests

The authors declare no competing or financial interests.

Author contributions

Conceptualization: K.T.; Methodology: A.Q., K.T.; Formal analysis: A.Q.; Investigation: A.Q., J.W.; Resources: K.T.; Writing - original draft: A.Q.; Writing - review & editing: A.Q., J.W., K.T.; Visualization: A.Q.; Supervision: K.T.; Funding acquisition: K.T.

Funding

This work was funded by the Canadian Cancer Society Research Institute (701936) and Natural Sciences and Engineering Research Council of Canada (05322-14).

Supplementary information

Supplementary information available online at
http://jcs.biologists.org/lookup/doi/10.1242/jcs.206979.supplemental

References

Anesten, F., Holt, M. K., Schéle, E., Pálsdóttir, V., Reimann, F., Gribble, F. M., Safari, C., Skibicka, K. P., Trapp, S. and Jansson, J.-O. (2016). Preproglucagon neurons in the hindbrain have IL-6 receptor-alpha and show Ca2+ influx in response to IL-6. *Am. J. Physiol. Regul. Integr. Comp. Physiol.* **311**, R115-R123.

Baker, D. J., Wijshake, T., Tchkonia, T., LeBrasseur, N. K., Childs, B. G., van de Sluis, B., Kirkland, J. L. and van Deursen, J. M. (2011). Clearance of p16Ink4a-positive senescent cells delays ageing-associated disorders. *Nature* **479**, 232-236.

Baker, D. J., Childs, B. G., Durik, M., Wijers, M. E., Sieben, C. J., Zhong, J., Saltness, R. A., Jeganathan, K. B., Verzosa, G. C., Pezeshki, A. et al. (2016). Naturally occurring p16(Ink4a)-positive cells shorten healthy lifespan. *Nature* **530**, 184-189.

Beck, C., Cayeux, S., Lupton, S. D., Dörken, B. and Blankenstein, T. (1995). The thymidine kinase/ganciclovir-mediated "suicide" effect is variable in different tumor cells. *Hum. Gene. Ther.* **6**, 1525-1530.

Bellocq, A., Suberville, S., Philippe, C., Bertrand, F., Perez, J., Fouqueray, B., Cherqui, G. and Baud, L. (1998). Low environmental pH is responsible for the induction of nitric-oxide synthase in macrophages. Evidence for involvement of nuclear factor-kappaB activation. *J. Biol. Chem.* **273**, 5086-5092.

Boulanger, M. J., Chow, D. C., Brevnova, E. E. and Garcia, K. C. (2003). Hexameric structure and assembly of the interleukin-6/IL-6 alpha-receptor/gp130 complex. *Science* **300**, 2101-2104.

Calabrese, L. H. and Rose-John, S. (2014). IL-6 biology: implications for clinical targeting in rheumatic disease. *Nat. Rev. Rheumatol.* **10**, 720-727.

Castro-Vega, L. J., Jouravleva, K., Ortiz-Montero, P., Liu, W.-Y., Galeano, J. L., Romero, M., Popova, T., Bacchetti, S., Vernot, J. P. and Londoño-Vallejo, A. (2015). The senescent microenvironment promotes the emergence of heterogeneous cancer stem-like cells. *Carcinogenesis* **36**, 1180-1192.

Childs, B. G., Durik, M., Baker, D. J. and van Deursen, J. M. (2015). Cellular senescence in aging and age-related disease: from mechanisms to therapy. *Nat. Med.* **21**, 1424-1435.

Coppé, J. P., Desprez, P.-Y., Krtolica, A. and Campisi, J. (2010). The senescence-associated secretory phenotype: the dark side of tumor suppression. *Annu. Rev. Pathol.* **5**, 99-118.

Cukusic, A., Ivankovic, M., Skrobot, N., Ferenac, M., Gotic, I., Matijasic, M., Polancec, D. and Rubelj, I. (2006). Spontaneous senescence in the MDA-MB-231 cell line. *Cell Prolif.* **39**, 205-216.

Edelstein, A. D., Tsuchida, M. A., Amodaj, N., Pinkard, H., Vale, R. D. and Stuurman, N. (2014). Advanced methods of microscope control using µManager software. *J. Biol. Methods* **1**, 10.

Guo, Q., Wang, X., Tibbitt, M. W., Anseth, K. S., Montell, D. J. and Elisseeff, J. H. (2012). Light activated cell migration in synthetic extracellular matrices. *Biomaterials* **33**, 8040-8046.

Hubackova, S., Kucerova, A., Michlits, G., Kyjacova, L., Reinis, M., Korolov, O., Bartek, J. and Hodny, Z. (2016). IFNgamma induces oxidative stress, DNA damage and tumor cell senescence via TGFbeta/SMAD signaling-dependent induction of Nox4 and suppression of ANT2. *Oncogene* **35**, 1236-1249.

Kalos, M., Levine, B. L., Porter, D. L., Katz, S., Grupp, S. A., Bagg, A. and June, C. H. (2011). T cells with chimeric antigen receptors have potent antitumor effects and can establish memory in patients with advanced Leukemia. *Sci. Transl. Med.* **3**, 95ra73.

Kokoris, M. S. and Black, M. E. (2002). Characterization of herpes simplex virus type 1 thymidine kinase mutants engineered for improved ganciclovir or acyclovir activity. *Protein Sci.* **11**, 2267-2272.

Liao, J. K., Seto, M. and Noma, K. (2007). Rho kinase (ROCK) inhibitors. *J. Cardiovasc. Pharmacol.* **50**, 17-24.

Luster, A. D., Alon, R. and von Andrian, U. H. (2005). Immune cell migration in inflammation: present and future therapeutic targets. *Nat. Immunol.* **6**, 1182-1190.

Journal of Cell Science

Mills, E. and Truong, K. (2011). Ca2+-mediated synthetic biosystems offer protein design versatility, signal specificity, and pathway rewiring. *Chem. Biol.* **18**, 1611-1619.
Mills, E., Pham, E., Nagaraj, S. and Truong, K. (2012). Engineered networks of synthetic and natural proteins to control cell migration. *ACS Synth. Biol.* **1**, 211-220.
Mosabbir, A. A. and Truong, K. (2017). Ca2+-mediated rewiring of cell homing and fusion to VEGF sources. *Cell Calcium*. **65**, 31-39.
Nagaraj, S., Mills, E., Wong, S. S. C. and Truong, K. (2013). Programming membrane fusion and subsequent apoptosis into mammalian cells. *ACS Synth. Biol.* **2**, 173-179.
Naghavi, M., John, R., Naguib, S., Siadaty, M. S., Grasu, R., Kurian, K. C., van Winkle, W. B., Soller, B., Litovsky, S., Madjid, M. et al. (2002). pH Heterogeneity of human and rabbit atherosclerotic plaques; a new insight into detection of vulnerable plaque. *Atherosclerosis* **164**, 27-35.
Ohkura, M., Sasaki, T., Kobayashi, C., Ikegaya, Y. and Nakai, J. (2012). An improved genetically encoded red fluorescent Ca2+ indicator for detecting optically evoked action potentials. *PLoS ONE* **7**, e39933.
O'Malley, D., Liston, M., Hyland, N. P., Dinan, T. G. and Cryan, J. F. (2011). Colonic soluble mediators from the maternal separation model of irritable bowel syndrome activate submucosal neurons via an interleukin-6-dependent mechanism. *Am. J. Physiol. Gastrointest. Liver Physiol.* **300**, G241-G252.
Qudrat, A. and Truong, K. (2017). Engineering Synthetic Proteins to Generate Ca2+ Signals in Mammalian Cells. *ACS Synth. Biol.* **6**, 582-590.
Rüegg, U. T. and Burgess, G. M. (1989). Staurosporine, K-252 and UCN-01: potent but nonspecific inhibitors of protein kinases. *Trends Pharmacol. Sci.* **10**, 218-220.
Saraswat, K. and Rizvi, S. I. (2017). Novel strategies for anti-aging drug discovery. *Expert Opin. Drug Discov.* **2**, 1-12.
Scheller, J., Chalaris, A., Schmidt-Arras, D. and Rose-John, S. (2011). The pro- and anti-inflammatory properties of the cytokine interleukin-6. *Biochim. Biophys. Acta* **1813**, 878-888.
Schneider, C. A., Rasband, W. S. and Eliceiri, K. W. (2012). NIH Image to ImageJ: 25 years of image analysis. *Nat. Methods* **9**, 671-675.
Smart, N., Mojet, M. H., Latchman, D. S., Marber, M. S., Duchen, M. R. and Heads, R. J. (2006). IL-6 induces PI 3-kinase and nitric oxide-dependent protection and preserves mitochondrial function in cardiomyocytes. *Cardiovasc. Res.* **69**, 164-177.
Tomicic, M. T., Thust, R. and Kaina, B. (2002). Ganciclovir-induced apoptosis in HSV-1 thymidine kinase expressing cells: critical role of DNA breaks, Bcl-2 decline and caspase-9 activation. *Oncogene* **21**, 2141-2153.
Van Overmeire, E., Stijlemans, B., Heymann, F., Keirsse, J., Morias, Y., Elkrim, Y., Brys, L., Abels, C., Lahmar, Q., Ergen, C. et al. (2016). M-CSF and GM-CSF receptor signaling differentially regulate monocyte maturation and macrophage polarization in the tumor microenvironment. *Cancer Res.* **76**, 35-42.
Wu, Y. I., Frey, D., Lungu, O. I., Jaehrig, A., Schlichting, I., Kuhlman, B. and Hahn, K. M. (2009). A genetically encoded photoactivatable Rac controls the motility of living cells. *Nature* **461**, 104-108.